Ferroelectricity and ferromagnetism of $La_{0.5}Lu_{0.5}Ni_{0.5}Mn_{0.5}O_3$ thin films on $Nb:SrTiO_3$ substrates

2010 J. Phys.: Condens. Matter 22 206005

(http://iopscience.iop.org/0953-8984/22/20/206005)

J. Phys.: Condens. Matter **22** (2010) 206005 (7pp) doi:10.1088/0953-8984/22/20/206005

Ferroelectricity and ferromagnetism of $La_{0.5}Lu_{0.5}Ni_{0.5}Mn_{0.5}O_3$ thin films on $Nb:SrTiO_3$ substrates

S Z Li[1,2], C Zhu[1,3], Z B Yan[1,3], S J Luo[1,3], K F Wang[1,3] and J-M Liu[1,3,4]

[1] Laboratory of Solid State Microstructures, Nanjing University, Nanjing 210093, People's Republic of China
[2] School of Physics, Hubei Normal University, Huangshi 435001, People's Republic of China
[3] International Center for Materials Physics, Chinese Academy of Sciences, Shenyang 110016, People's Republic of China

E-mail: liujm@nju.edu.cn

Received 29 December 2009, in final form 9 April 2010
Published 30 April 2010
Online at stacks.iop.org/JPhysCM/22/206005

Abstract

Epitaxial orthorhombic $La_{0.5}Lu_{0.5}Ni_{0.5}Mn_{0.5}O_3$ (LLNMO) thin films deposited on $Nb:SrTiO_3$ (NSTO) substrates are prepared by pulsed laser deposition and their ferroelectricity and magnetism are investigated using various techniques. It is revealed that the as-prepared thin films are ferromagnetic (FM) insulators. The FM transition occurring at ~125 K is evidenced by the well defined hysteresis at low temperature, with a saturated magnetic moment as high as 1.8 μ_B/f.u. at ~5 K. A reversible ferroelectric polarization of ~0.2 μC cm^{-2} below ~140 K is also observed. The magnetism can be understood by the FM ordering associated with a partially ordered major Ni^{2+}–Mn^{4+} plus minor Mn^{3+}–Ni^{3+} configuration, while the ferroelectricity is argued to originate from the A-site disordering of La^{3+} and Lu^{3+}.

(Some figures in this article are in colour only in the electronic version)

1. Introduction

Multifunctional materials combining magnetism and ferroelectricity have been attracting increasing attention. These materials can be used to encode binary data in an advanced manner in ferroelectric and magnetic random access memories etc [1–3]. For better application, the coexistence of ferromagnetic (FM) and ferroelectric (FE) properties must be addressed and furthermore a coupling between the FM and FE orders would also be preferred. Such a coexistence and coupling may be reachable in magnetic perovskite oxides such as ferrites ($BiFeO_3$, $BiMnO_3$) and manganites ($RMnO_3$, R = Tb, Dy, Ho etc), as has been extensively investigated [3–5]. Some of these oxides give only weak magnetic moment and magnetoelectric (ME) coupling, others require an extraordinary synthesis strategy. Therefore, searching for novel materials with good ferroelectricity and ferromagnetism as well as ME coupling remains a challenge to materials researchers.

Recently, another class of complex oxide compounds, magnetic perovskite oxides $A_2BB'O_6$ ($AB_{0.5}B'_{0.5}O_3$), have been synthesized and characterized. Here the A-site refers to Bi or rare earth element R (R = La–Lu and Y) and the B (B′)-site often refers to Mn, Ni, Co and Cr etc. Structurally, $A_2BB'O_6$ consists of alternatively arranged B/B′ in the ideal ABO_3 unit cell, leading to a long-ranged ordered double perovskite. For $AB_{0.5}B'_{0.5}O_3$, it shows a random distribution of B/B′ in a pseudoperovskite ABO_3 with a fully disordered unit cell. Investigations on ceramic and thin film La_2NiMnO_6 (LNMO) and La_2CoMnO_6 (LCMO) revealed that they are insulators of high resistivity, and the thin film magnetism shows significant substrate-dependence, in particular for the case of large lattice mismatch between the thin films and substrates [6–12]. These materials are expected to offer promising ferroelectricity and preferred magnetism at room temperature and thus are potential multiferroic candidates for device applications.

Because of ferromagnetism requirement for enhanced multiferroicity, the magnetic structure of these materials has

[4] Author to whom any correspondence should be addressed.

been intensively investigated [7, 12]. For fully disordered LNMO with chemical formula $LaNi_{0.5}Mn_{0.5}O_3$, the Ni and Mn cations distribute randomly at the B(B′)-site. Such a random distribution results in Ni–O–Mn, Ni–O–Ni, and Mn–O–Mn chemical bonds with different superexchange interactions. The Ni–O–Ni and Mn–O–Mn bonds are expected to exhibit ferromagnetic (FM) superexchange interactions and antiferromagnetic (AFM) superexchange interactions, respectively. Their presence hinders the formation of long-range FM order arising from the FM interaction of the Ni–O–Mn bonds, leading instead to a quite low FM transition temperature (T_c). In order to enhance the FM order, fully ordered Ni/Mn occupation at the B(B′)-site is thus preferred, although practically it is difficult to reach by conventional synthesis approach. Due to the Goodenough–Kanamori rules, such an order structure may offer both FM and insulating behaviors, both highly preferred for good multiferroicity. In such a case, the FM order arises from the 180°-superexchange interaction between the two transition metal cations [6, 7, 13, 14].

Also, theoretical calculation predicts that an ordered Ni^{2+}–Mn^{4+}/Ni^{3+}–Mn^{3+} configuration at the $B(B')$-site in LNMO contributes largely to the magnetic moment, i.e. ferromagnetism [7, 8]. Therefore, from the magnetic consideration, LNMO cannot offer good ferromagnetism unless such an ordered configuration is sufficiently maintained. Nevertheless, neutron diffraction experiments on the valence of Ni and Mn ions in LNMO by various groups gave contradictory results: either the presence of Ni^{2+} and Mn^{4+} or the presence of Ni^{3+} and Mn^{3+} at the B-site [15–22]. This implies that the occupation of Ni/Mn at the B-site may be partially ordered rather than fully ordered in either the Ni^{2+}/Mn^{4+} or Ni^{3+}/Mn^{3+} form, which is unfavorable for enhanced multiferroicity. To overcome this problem, Gupta *et al* investigated the effect of deposition parameters for thin film LNMO on the magnetism, and revealed that the optimization of the deposition parameters can lead to ferromagnetism with high T_c [7, 8], as confirmed subsequently by Kitamura *et al* [12]. Although subsequent Raman spectroscopy and transmission electron microscopy demonstrated that these films are somehow of short-range Ni/Mn order [8, 11], there is the possibility to manipulate the magnetism by controlling the deposition parameters for thin film LNMO.

More interesting is the recent investigation on ferroelectricity in LNMO-based materials. First-principles calculations predict the presence of electric dipoles in A-site disordered double perovskite $(LaLu)(NiMn)O_6$ (LLNMO) with a Lu concentration of ∼50% [23], indicating that the A-site doping may benefit the generation of ferroelectricity. The underlying mechanism is associated with the well known fact that ferroelectricity can be generated in perovskite oxides with small and off-centered A-site ions although the tolerance factor $t = (r_O + r_A)/\sqrt{2}(r_O + r_B)$, where r_O, r_A and r_B are the ionic radii of oxygen, A-site, and B-site ions, respectively, may be less than one ($t \sim 0.84$ for LLNMO where Lu is much smaller than La). This prediction allows the possibility to synthesize novel materials by doping at the A-site of LNMO with small rare earth ions or other 3+ small ions, because the A-site doping may lead to ferroelectricity and the B(B′)-site ordered Ni/Mn configuration (even partially) may lead to ferromagnetism, and hence the coexistence of ferroelectricity and ferromagnetism. This is the major motivation for the present work.

Nevertheless, it should be mentioned that LLNMO is hard to synthesize because of phase competition and separation [24]. LLNMO in bulk form exhibits a mixed microstructure at room temperature (T), composed of a rhombohedral structure ($R\bar{3}$) and hexagonal structure [6], which definitely causes additional complexity for achieving good multiferroicity. One way to avoid this mixture is to prepare LLNMO thin films with a symmetry confined by the substrate symmetry. This confined symmetry may be orthorhombic if the substrate is $SrTiO_3$, and a similar strategy was reported for epitaxial La_2NiMnO_6 thin films on $SrTiO_3$ [7, 10]. Also, the conditions for thin film preparation should be optimized so that the B-site Ni^{2+}/Mn^{4+} order obtained is as great as possible, in order to enhance the ferromagnetism.

In this work, we thus report our efforts to prepare orthorhombic LLNMO thin films on Nb:$SrTiO_3$ (NSTO) substrates using pulsed laser deposition (PLD). We shall demonstrate that the as-prepared thin films under optimized deposition conditions do exhibit ferromagnetism and reversible FE polarization, both at relatively high T. By various characterizations we argue that the as-prepared thin films have A-site disordered cations and the B(B′)-site mainly possesses Ni^{2+}/Mn^{4+} order, both beneficial to the measured ferromagnetism and ferroelectricity.

2. Experimental details

The PLD experiment was performed using a KrF excimer laser with a wavelength of 248 nm and a pulse width of 25 ns. The ceramic LLNMO target was synthesized using a conventional solid-sintering method and it is a mixture of rhombohedral $LaNiO_3$ and hexagonal $LuMnO_3$. Commercially available (001)-NSTO wafers were used as substrates. An excimer laser beam of 3 Hz in rep-rate and ∼2.0 J cm^{-2} in energy density was used. During the deposition, the substrate temperature was 800 °C with variable oxygen pressure, the optimized pressure in terms of the structural quality and ferroelectricity/magnetism is 12 Pa. The as-prepared thin films, ∼450 nm in thickness, were *in situ* annealed at the same temperature in ambient oxygen of $\sim 10^4$ Pa for 15 min to improve the crystallinity and reduce oxygen defects.

For the microstructural characterization, x-ray θ–2θ diffraction (XRD) and pole-figure analysis with a X'Pert Pro HRXRD apparatus were used to check the crystalline quality of the as-prepared thin films. Transmission electron microscopy (TEM) with aberration correction (JEM4000) was performed in addition to identify the thin film microstructure. The TEM specimens were prepared by conventional grinding and milling. To check the octahedral B–O stretching vibrations, Raman spectroscopy was undertaken using a JY-HR800 microscope with an Ar ion laser (546 nm) source. The laser beam was focused down to a spot size of several microns in

diameter using a microscope objective normal to the substrate surface. The emitted light was dispersed by a 1800 mm^{-1} grating.

The species valences of the as-prepared thin films were checked using x-ray photoemission spectroscopy (XPS) with an Al Kα source ($h\nu$ = 1486.6 eV) with the Thermo ESCALAB 250. For the XPS probing, both the surface detection and depth-profile analysis were pre-employed. For the depth-profile analysis, the Ar ion beam was used to remove the surface layer. However, our experiments revealed that such a procedure seemed to impact the valence of some species. In particular, the Ni^{3+} and Mn^{3+} ions, which are both in 3+, were transformed into Ni^{2+}/Ni and Mn^{4+} ions by the ion-beam irradiation. Therefore, in this work, only the surface analysis on the very fresh thin film samples was used for the XPS experiments, and the sample-to-sample data show quite good consistency between them.

For the physical property characterization, we employed various techniques. For the magnetic measurement, a superconducting quantum interference device (SQUID, Quantum Design Inc.) was used. Since the NSTO substrates have significant diamagnetism, a careful subtraction of the magnetic signals of the thin film from those of the substrate plus thin film becomes critical. We first performed the required measurements on the NSTO substrate, such as magnetization (M)–magnetic field (H) hysteresis and M–temperature (T) relation, and then did the same measurements on the thin film plus substrate. Finally, the data on the magnetism of the thin films were subtracted by point-to-point comparison between the data from the substrate sample and the thin film plus substrate sample. The magnetic measurements were performed in both the standard field-cooling (FC) and zero-field-cooled (ZFC) modes. For example, the M–H hysteresis was measured at a given T after the sample was cooled from high T under the FC and ZFC conditions.

For the dielectric and FE measurements, Au electrodes, each 1.0 mm^2 in area, were sputtered onto the surface of the thin film and welded to fine copper wires with Ag glue. The dielectric susceptibility was probed using an HP4294A impedance analyzer connected to a physical properties measurement system (PPMS, Quantum Design Inc.) and a CTI-Cryogenics unit. Here, the great care was paid to the measurement of the FE polarization P, which was probed by the pyroelectric current method using a Keithley 6514 electrometer, also connected to the PPMS. During the measurement, the thin films under an electric field E = 111 kV cm^{-1} or -111 kV cm^{-1} were cooled down to T = 20 K. This corresponds to the electric poling process. Then the electric field was removed and followed by a sufficiently long duration short-circuit procedure. The pyroelectric current was measured during the warming sequence, starting from T = 20 K at several rates from 1 to 3 K min^{-1}, to exclude the contribution from the thermally de-trapped charges; note that this measuring method does not allow any leakage current since no electric field was imposed on the samples during the pyroelectric current measurement.

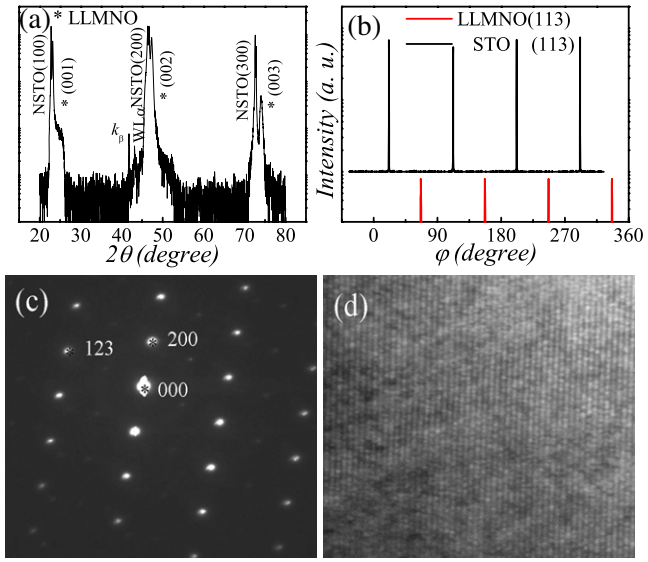

Figure 1. (a) θ–2θ XRD of the as-prepared LLNMO thin film deposited on the (001) Nb:$SrTiO_3$ substrate. (b) φ-scan of the (113) peaks for orthorhombic LLMNO and $SrTiO_3$ substrate. (c) Electric diffraction pattern along the [011] axis and (d) high-resolution TEM image of the LLNMO thin film.

3. Results and discussions

3.1. Orientation of growth of LLNMO thin film

First, we prepared a series of thin films under various deposition conditions, mainly by varying the substrate temperature and oxygen pressure for deposition. It is shown that a substrate temperature lower than 800 °C led to an inhomogeneous structure with an impurity phase and a higher temperature led to a large leakage current. On the other hand, a lower pressure of ambient oxygen always led to a large leakage current, probably due to the oxygen vacancies in the thin films, and a higher pressure of ambient oxygen often resulted in some impurity. In our experiments, the optimized deposition conditions are 800 °C for the substrate temperature and 12 Pa for the oxygen pressure.

The XRD θ–2θ spectrum of the as-prepared thin films under the optimized deposition conditions is shown in figure 1(a). It is seen that the LLNMO thin film is completely (001) oriented and no other impurities or reflections are identified, indicating a coherent structural match between the film and substrate. The epitaxial relationship between the thin film and substrate was further confirmed by XRD pole-figure analysis using the φ-scan mode, referring to the (113) orientations of LLMNO and STO, as shown in figure 1(b). Four (113) reflections with 90° separation from the thin film and the STO were observed, indicating the epitaxial coherent growth of the film on the substrate.

To better understand the microstructure of the thin film, selected area electric diffraction (SAED) along the [011]-axis of the thin film is given in figure 1(c). It is confirmed that the film is single-phased, without an impurity phase, but the distorted spots probably reflect the existence of strain in the thin film. Figure 1(d) shows the high-resolution TEM

image (HRTEM), again illustrating the high quality and single-phase structure, whereas the (220)/(022) imaging hints at weak lattice distortion. Combining the XRD spectrum with the SAED/HRTEM patterns leads to the conclusion that the LLNMO thin films deposited on NSTO substrates favor the room temperature meta-stable orthorhombic structure with a slight lattice strain over the films.

Theoretically, the out-of-plane lattice mismatch between the film and substrate is ∼2.2% and the as-generated strain in the film would be quite significant even though the film is ∼450 nm in thickness. This allows one to argue that the film is strained and the strain distribution along the out-of-plane direction is partially relaxed and thus inhomogeneous. In fact, an earlier report confirmed the existence of strain in thin films of ∼100 nm and over in thickness [25], and a gradient of strain as a function of thickness is expected [26]. Similar results were reported for LNMO thin films with a similar structure to the present LLMNO thin films [8]. This strain gradient would have an impact on the magnetism and ferroelectricity of the thin films, to be addressed later.

We also performed Raman spectroscopy to probe the structural distortion (not the substrate induced strain) of the LLNMO thin films with respect to LNMO (no Lu-doping) thin films on NSTO substrates. It is observed that the A_g and B_{2g} modes associated with the octahedral B–O stretching vibrations shift respectively toward ∼507 (A_g) and ∼653 cm^{-1} (B_{2g}) from ∼538 (A_g) and ∼683 cm^{-1} (B_{2g}) for LNMO thin film [11]. This significant blue-shift reflects that the domains in the LLNMO thin film have different degrees of Ni–Mn order from those in LNMO, which results in different contributions to the B–O stretching bands, noting that LLMNO has a smaller tolerance factor because of the Lu^{3+} doping, which leads to the change of the arrangement for MnO_6 and NiO_6.

3.2. X-ray photoelectron spectroscopy

To reveal the physics underlying the magnetism in LLNMO thin films, it is essential to probe the species valences so as to clarify whether either Ni^{2+}–Mn^{4+} or Ni^{3+}–Mn^{3+} contributes to the ferromagnetism. The XPS data from the surface layer of the as-prepared LLNMO thin film are shown in figures 2(a)–(e), where the valence band energy (VBE) and corresponding core-level spectra of Mn 2p, Ni 2p, Ni 3p, Lu 4f and La 3d are presented. It should be noted again that the XPS data were collected from the surface layer of the fresh samples, while a depth-profile XPS analysis was not possible due to the valence fluctuations induced by the ion-beam irradiation in order to remove the surface layer.

First, the 2p core-level spectra of Mn shown in figure 2(a) indicate that the binding energy (BE) of the $2p_{1/2}$ peak for MnO_2 and Mn_2O_3 is 654.1 and 653.6 eV, respectively. Therefore, the difference between the BEs of Mn $2p_{3/2}$ implies that the oxidation state of Mn is composed of mixed Mn^{4+} and Mn^{3+}. Figure 2(b) shows the 2p core-level spectra of Ni. The binding energy of the satellite peak of La $3d_{3/2}$ is almost identical to the BE of $2p_{3/2}$ of Ni in the oxide state, usually for compounds containing both La and Ni these peaks overlap each other, while the intensity of secondary peak is stronger

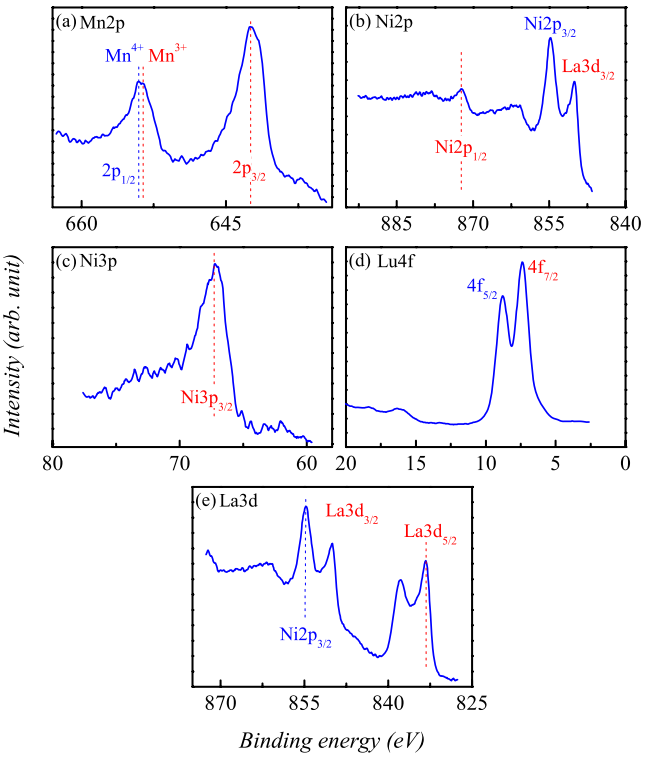

Figure 2. XPS spectra of the LLNMO thin film: (a) Mn 2p XPS spectra, (b) Ni 2p XPS spectra, (c) Ni 3p XPS spectra, (d) and (e) Lu 4f and La 3d spectra, respectively.

than that of the main peak for La $3d_{3/2}$. One thus needs more data to identify the dominant valence state of Ni.

To do this, i.e. to distinguish the BEs of NiO and Ni_2O_3, we analyze the 3p core-level for Ni, as shown in figure 2(c). Quite clearly, the BE is ∼67.2 eV, similar to that for NiO [27]. This indicates that the Ni valence in the thin film is mainly Ni^{2+}. On the other hand, it was reported that the Ni $2p_{3/2}$ BE in Ni_2O_3 containing low-spin Ni^{3+} is lower than that in NiO containing Ni^{2+} [28].

Finally, inspecting the BEs of Lu 4f and La 3d, as shown in figures 2(d) and (e), allows a determination of Lu^{3+} and La^{3+} in the thin film because the spectra are essentially the same as the data recorded in handbook for BE of XPS [29]. Therefore, it is safe to conclude that the Ni^{2+}–Mn^{4+} pairs dominate in the as-prepared LLNMO thin film.

3.3. Ferromagnetism

Given the single-phase evidence and the knowledge on the species valences, we are in a good position to understand the magnetism. By carefully subtracting the magnetic signal of the thin film from the substrate contribution, as mentioned in section 2, we present in figure 3(a) the measured M as a function of T under ZFC and FC (at $H = 1000$ Oe) conditions, while H is applied parallel to the film surface. The measured M in the ZFC case exhibits a clear FM transition at $T \sim 125$ K from the high-T paramagnetic state, as defined by fitting to the Curie–Weiss law, and the transition does not end until $T \to 0$, characterized by an almost saturated M at $T \to 0$ K.

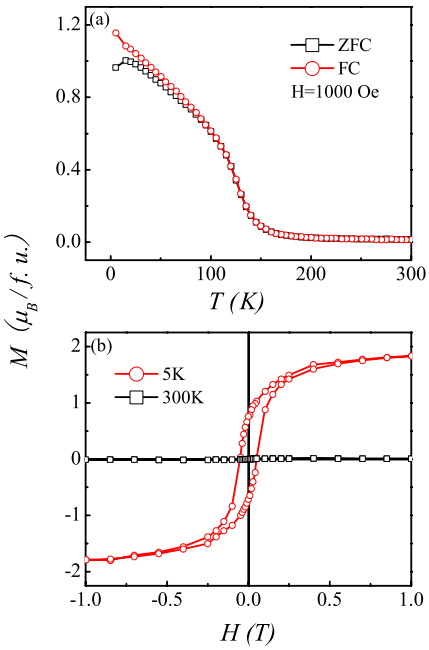

Figure 3. (a) Measured M–T curve with $H = 1000$ Oe under ZFC and FC conditions, where H is applied parallel to the thin film. (b) Measured M–H hysteresis at $T = 5$ K and 300 K, respectively.

Furthermore, the measured M–T data in the FC case do not show a remarkable difference from the ZFC data, only a slight gap between the two sets of data appears at $T \sim 80$ K and below. This indicates that the transitions seem to be dominated by FM ordering while the contribution from the spin-glass-like ingredient, if any, is not significant.

We also obtain the M–H hysteresis of the thin film under the ZFC conditions (i.e. the M–H hysteresis is measured at T after cooling from room temperature in the ZFC mode), and the data at $T \sim 5$ and 300 K are shown in figure 3(b). The loop at ∼5 K is well saturated with a coercivity of 500 Oe and a saturated moment of 1.8 μ_B/formula unit (f.u.). This moment, even smaller than the theoretical spin-only moment of 5 μ_B/f.u., indicates that the spin configuration of the LLNMO thin film is mainly ferromagnetically ordered, while the spin-glass or AFM-dominant spin configuration alone could not possibly produce such a large and saturated moment. If the spin configuration consists of an FM phase in coexistence with a spin-glass phase, a fully saturated moment (5 μ_B/f.u.) would be also hard to reach. In addition, it should be mentioned that the inhomogeneous strain in the thin film might also contribute to the magnetism by partially suppressing the saturated moment. However, an earlier report [8] indicated that this effect, if it exists, should not be significant and details of it are reserved for further investigation. By the way, the M–H loop above ∼140 K becomes very small, predicting a paramagnetic state above ∼140 K.

This strong FM order may originate from the structure-dependent spin interactions in the LLNMO thin films. As mentioned earlier, the Kanamori–Goodenough FM superexchange interaction between the ordered Ni^{2+}–Mn^{4+} and/or Ni^{3+}–Mn^{3+} configuration contributes to the FM order, while the XPS data revealed that the major configuration in the LLNMO thin films is Ni^{2+}–Mn^{4+}, with the Ni^{3+}–Mn^{3+} configuration being minor. This allows us to argue that the probed FM moment of the LLNMO thin films is mainly from the partially ordered Ni^{2+}–Mn^{4+} configuration plus a minor Ni^{3+}–Mn^{3+} alignment. This FM interaction is particularly strong because of the strong coupling via the e_g–p_σ hopping through the almost linear Ni–O–Mn bonds. Second, with respect to LNMO, whose FM ordering occurs at ∼280 K with a saturated moment of ∼4.04 μ_B/f.u. [7] and ∼4.8 μ_B/f.u. [30], LLNMO has a much lower FM transition point and a smaller saturated moment, indicating that the substitution of La with Lu has a significant impact on the spin ordering sequence. The reason lies in the fact that Lu^{3+} has smaller ionic radius than La^{3+}. A smaller A-site size usually results in a lower FM ordering point [6], since a smaller tolerance factor t corresponds to a more distorted arrangement of NiO_6 and MnO_6 octahedra. It is also reasonable to argue that thin film samples are usually accommodated with higher oxygen vacancies and more disordered Mn^{4+}–Ni^{2+} and Mn^{3+}–Ni^{3+} pairs.

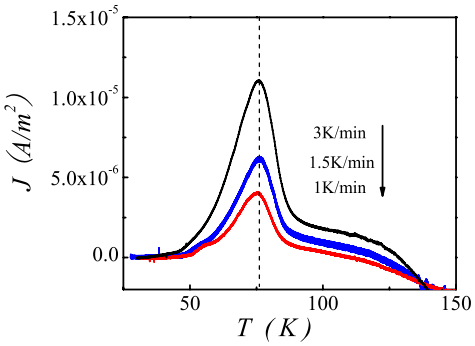

Figure 4. Measured electric current density J of the as-prepared LLNMO thin film as a function of T, recorded in the warming sequence, with different ramp rates: 3, 1.5, and 1.0 K min^{-1}, after cooling the sample under an external electric field $E = 111$ kV cm^{-1} applied below 160 K.

3.4. Dielectric and ferroelectric behaviors

Subsequently, we investigate the dielectric and FE behaviors of the as-prepared LLNMO thin films. The dielectric constant as a function of T over a broad frequency range is measured. The T- and frequency dependencies of the dielectric constant are similar to those of other double perovskites, such as La_2MnNiO_6 and La_2CoMnO_6 [14, 31], and no other special property for the LLNMO thin films needs to be addressed here. Detailed analysis on the modulus Z and loss angle θ of the impedance at low T shows that the sample behaves as a pure capacitor.

We pay our major attention to the ferroelectricity. We measure the T-dependence of the measured polarization P using the pyroelectric current method [32]. It should be mentioned that above ∼250 K the thermally activated trapped charges become dominant and the data obtained with different warming ramp rates show a difference. However, below $T = 160$ K, the thermally activated charge flow is negligible, and an example is shown in figure 4, where the measured current J as

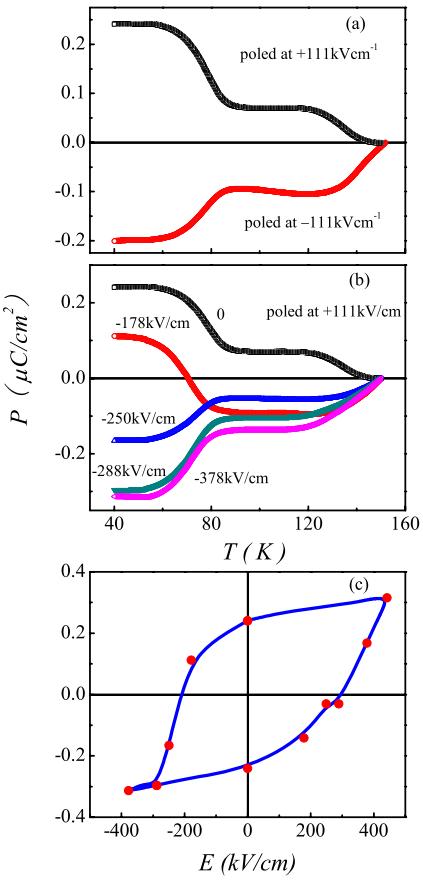

Figure 5. (a) Measured P–T curves under a positive field $E = 111$ kV cm^{-1} and a negative field $E = -111$ kV cm^{-1}. (b) Measured P–T curves upon various switching field E_n (numerically labeled) after a previous poling by a positive field $E_p = 111$ kV cm^{-1}. (c) Evaluated P–E hysteresis at $T = 40$ K.

a function of T was measured at three different warming ramp rates: 3 K min^{-1}, 1.5 K min^{-1}, and 1.0 K min^{-1}, respectively. It is found that the peak of the J–T curve does not shift along the T-axis, and the integration of $J(t)$ over the three curves remain similar in each case. This indicates that de-trapped charges, if any, do not contribute much to the measured current and the pyroelectric current is dominant.

The measured polarization results are presented in figure 5(a). The measured P as a function of T under $H = 0$ shows two plateaus: P ensues at $T \sim 140$ K and then increases rapidly up to a plateau with decreasing T, subsequently there is a further increase from $T \sim 90$ K up to the second plateau. While the appearance of the first plateau indicates the onset of ferroelectric ordering, the second plateau may be relevant to the magnetic ordering, bearing in mind that the FM transitions end roughly at $T \sim 90$ K, as shown by the $M(T)$ curve in figure 3(a). Certainly, clarification of the relevance of this needs further evidence and the underlying mechanism also requires additional investigation.

To confirm the ferroelectricity of the LLNMO thin film, one has to demonstrate the reversal of P driven by an external electric field. Take the case performed at $T = 40$ K as an example. To better settle this problem and make sure that the data are reliable, we first pole the sample at $T = 160$ K with a sufficiently high positive $E_p = 111$ kV cm^{-1} and then cool it down to $T \sim 40$ K under E_p. Then we turn off E_p and re-apply a negative field E_n (i.e. switching field, $E_n = 0$–-400 kV cm^{-1}) to the sample for at least 10 min before turning it off, followed by a sufficiently long time for short-circuit, at $T \sim 40$ K. Finally, we probe the pyroelectric current during the warming process. The measured $P(T)$ data under different E_n values are plotted in figure 5(b).

It is clearly shown in figure 5(b) that polarization P is reversed once $E_n >\sim 250$ kV cm^{-1}. This polarization reversal sequence can be repeated if a positive field $E_p \sim 250$ kV cm^{-1} or higher one is applied again. The maximum P is about 0.2 μC cm^{-2} and the FE transition is evidenced at $\sim$140 K. This reversible polarization satisfies the ferroelectric criteria [33]. From the measured data, one can obtain the $P-E$ hysteresis loop, as shown in figure 5(c), which allows us to claim that the as-prepared LLNMO thin film is ferroelectric below $\sim$140 K. Therefore, we demonstrate the simultaneous existence of both FM and FE behaviors below $\sim$90 K in the as-prepared LLNMO thin films.

To understand the origin of the ferroelectricity, we address the A-site size disorder in LLNMO. First-principles calculations suggest that the octahedral tilting in (Li, K)NbO_3 with an average tolerance factor much smaller than one is prevented, because K ions and smaller Li ions are distributed randomly in the lattice; this is coined as A-site disorder. The ferroelectricity originates from the large off-centering of Li ions, contributing significantly to the difference between the tetragonal and rhombohedral ferroelectric states and yielding a tetragonal ground state even without strain coupling [34]. This scenario allows us to argue for a similar origin for the ferroelectricity in LLNMO where the polar-type lattice distortion is induced. This polar behavior arises from the frustration of the octahedral tilting instabilities due to the mixture of A-site cations of different sizes (La^{3+} ions and Lu^{3+} ions) and the fact that the coherence length for the A-site off-centering is shorter than that for the tilting instabilities [15].

We should mention here the effect of strain on the ferroelectricity of the thin film. Because the strain along the out-of-plane direction is inhomogeneous, the polarization P across the thin film is also inhomogeneous. Due to the fact that the strain is compressive, one has reason to argue that the gradient of P normal to the film surface is opposite to the gradient of the strain, noting that compressive strain usually suppresses polarization [35], although direct evidence for this argument is needed.

We have shown that the as-prepared LLNMO thin films offer both ferromagnetism and ferroelectricity at relatively high temperature. The ferromagnetism originates mainly from the partially ordered Ni^{2+}–Mn^{4+} plus a minor Ni^{3+}–Mn^{3+} configuration at the B-site, while the ferroelectricity is argued to result from the A-site disordered La^{3+}–Lu^{3+} configuration. The underlying mechanism seems similar to $BiFeO_3$, in which the magnetism and ferroelectricity come from different lattice sites. Therefore, a relatively weak coupling between the two types of orders is expected. In fact, our experiments confirmed this argument, and the polarization response to external magnetic field is insignificant. However, due to

the A-site Lu-doping induced lattice distortion and the A-site disordering, the spin–lattice coupling allows suppression of the magnetism, which should on reversal result in variation of the polarization by external magnetic field. Therefore, further investigations on the ME effect are needed.

4. Conclusions

In summary, we have prepared *c*-axis epitaxial LLNMO thin films on (001) NSTO substrates by pulsed laser deposition. The measured data on the magnetism and ferroelectricity confirm the coexistence of ferroelectricity and ferromagnetism at a relatively high temperature. Ferroelectric reversal driven by external electric field has been realized. It is also suggested that the Ni^{2+}–Mn^{4+} pairs dominate in the thin film, and are responsible for the ferromagnetism, but the A-site disorder suppresses the FM ordering tendency. We discuss the possible origins for the ferroelectricity and ferromagnetism, and suggest that A-site size disorder with different ions is responsible for the ferroelectricity while the ferromagnetism is mainly from Ni^{2+}–Mn^{4+} pairs.

Acknowledgment

This work was supported by the Natural Science Foundation of China (10874075, 50832002), the National Key Projects for Basic Research of China (2009CB623303, 2009CB929501), and the Natural Science Foundation of Jiangsu Province, China (BK2008024).

References

[1] Hur N, Park S, Sharma P A, Ahn J S, Guha S and Cheong S-W 2004 *Nature* **429** 392
[2] Ramesh R and Spaldin N A 2007 *Nat. Mater.* **6** 21
[3] Wang K F, Liu J-M and Ren Z F 2009 *Adv. Phys.* **58** 321
[4] Eerenstein W, Morrision F D, Scott J F and Mathur N D 2005 *Appl. Phys. Lett.* **87** 101906
[5] Kimura T, Kawamoto S, Yamada I, Azuma M, Takano M and Tokura Y 2003 *Phys. Rev.* B **67** 180401
[6] Dass R I and Goodenough J B 2003 *Phys. Rev.* B **67** 014401
[7] Padhan P, Guo H Z, LeClair P and Gupta A 2008 *Appl. Phys. Lett.* **92** 022909
[8] Guo H Z, Burgess J, Ada E, Street S and Gupta A 2008 *Phys. Rev.* B **77** 174423
[9] Hashisaka M, Kan D, Masuno A, Takano M, Shimakawa Y, Terashima T and Mibu K 2006 *Appl. Phys. Lett.* **89** 032504
[10] Guo H Z, Gupta A, Calvarese T G and Subramanian M A 2006 *Appl. Phys. Lett.* **89** 262503
[11] Guo H, Burgess J, Street S, Gupta A, Calvarese T G and Subramanian M A 2006 *Appl. Phys. Lett.* **89** 022509
[12] Kitamura M, Ohkubo I, Kubota M, Matsumoto Y, Koinuma H and Oshima M 2009 *Appl. Phys. Lett.* **94** 132506
[13] Joseph Joly V L, Joy P A, Date S K and Gopinath C S 2002 *Phys. Rev.* B **65** 184416
[14] Rogado N, Li J, Sleight A W and Subramanian M A 2005 *Adv. Mater.* **17** 2225
[15] Blasco J, Sanchez M C, Perez-Cacho J, Garcia J, Subias G and Campo J 2002 *J. Phys. Chem. Solids* **63** 781
[16] Bull C L, Gleeson D and Knight K S 2003 *J. Phys.: Condens. Matter* **15** 4927
[17] Iliev M N, Guo H and Gupta A 2007 *Appl. Phys. Lett.* **90** 151914
[18] Singh M P, Grygiel C, Sheets W C, Boullay Ph, Hervieu M, Prellier W, Mercey B, Simon Ch and Raveau B 2007 *Appl. Phys. Lett.* **91** 012503
[19] Zhou S M, Shi L, Yang H P and Zhao J Y 2007 *Appl. Phys. Lett.* **91** 172505
[20] Kitamura M, Ohkubo I, Matsunami M, Horiba K, Kumigashira H, Matsumoto Y, Koinuma H and Oshima M 2009 *Appl. Phys. Lett.* **94** 262503
[21] Guo H Z, Gupta A, Varela M, Pennycook S and Zhang J D 2009 *Phys. Rev.* B **79** 172402
[22] Truong K D, Singh M P, Jandl S and Fournier P 2009 *Phys. Rev.* B **80** 134424
[23] Singh D J and Park C H 2008 *Phys. Rev. Lett.* **100** 087601
[24] Park S, Hur N, Guha S and Cheong S W 2004 *Phys. Rev. Lett.* **92** 167206
[25] Ranno L, Llobet A, Tiron R and Favre-Nicolin E 2002 *Appl. Surf. Sci.* **188** 170
[26] Nix W D and Gao H J 1998 *J. Mech. Phys. Solids* **46** 411
[27] Mclntyre N S and Cook M G 1975 *Anal. Chem.* **47** 2208
[28] Ng K T and Hercules D M 1976 *J. Phys. Chem.* **80** 2094
[29] Moudler J F, Stickle W F, Sobol P E and Bomben K D 1992 *Handbook of X-Ray Photoelectron Spectroscopy* (Eden Prairie, MN: Perkin-Elmer)
[30] Singh M P, Truong K D, Jandl S and Fournier P 2009 *Phys. Rev.* B **79** 224421
[31] Singh M P, Truong K D and Fournier P 2007 *Appl. Phys. Lett.* **91** 042504
[32] Kimura T, Sekio Y, Nakamuba H, Siegrist T and Ramirez A P 2008 *Nat. Mater.* **7** 291
[33] Lines M E and Glass A M 1979 *Principles and Applications of Ferroelectrics and Related Materials* (Oxford: Clarendon)
[34] Saito Y, Takao H, Tani T, Nonoyama T, Takatori K, Homma T, Nagaya T and Nakamura M 2004 *Nature* **432** 84
[35] He F Z, Wells B O and Shapiro S M 2005 *Phys. Rev. Lett.* **94** 176101